Homologous Recombination and Non-Homologous End Joining are Mutually Exclusive in Ionizing Radiation Protection

Stefan J. Roobol[1,2,3], Sigrid Swagemakers[4,5], Yanto Ridwan[1,3], Paula van Heijningen[1], G. van de kamp[1], T. Heemskerk[1], C. Roland Wolf[6], George Garinis[7], Christophe Badie[8], Roland Kanaar[1,2], Dik C. van Gent[1,2] and Jeroen Essers[1,9,10,*]

[1]*Department of Molecular Genetics,* [2]*Oncode Institute, Erasmus University Medical Center, Rotterdam, The Netherlands*

[3]*Department of Radiology & Nuclear Medicine, Erasmus University Medical Center, Rotterdam, The Netherlands*

[4]*Department of Pathology, Erasmus University Medical Center, Rotterdam, The Netherlands*

[5]*Department of Bioinformatics, Erasmus University Medical Center, Rotterdam, The Netherlands*

[6]*Department of Systems Medicine, School of Medicine, University of Dundee, Ninewells Hospital, Dundee, United Kingdom.*

[7]*Institute of Molecular Biology and Biotechnology, Foundation for Research and Technology-Hellas, Nikolaou Plastira 100, 70013, Heraklion, Crete, Greece*

[8]*Cancer Mechanisms and Biomarkers Group, Radiation Effects Department, Centre for Radiation, Chemical and Environmental Hazards, Public Health England, Chilton, Didcot, United Kingdom.*

[9]*Department of Radiation Oncology, Erasmus University Medical Center, Rotterdam, The Netherlands*

[10]*Department of Vascular Surgery, Erasmus University Medical Center, Rotterdam, The Netherlands*

**Correspondence*

Jeroen Essers: j.essers@erasmusmc.nl

Manuscript in preperation

ABSTRACT

Ionizing radiation (IR) induced DNA damage activates many pathways which are crucial to preserve genome integrity. One of the most toxic type of DNA damage is the Double Strand Break (DSB), which can be repaired by at least two different DNA repair pathways, Non-Homologous End Joining (NHEJ) and Homologous Recombination (HR). Here we combined deletion of DNA-PK_{cs}, which has a role in NHEJ, with the disruption of HR gene *RAD54* to investigate the possible interplay of two distinct DSB repair pathways. Disrupting *RAD54* in mice with a *DNA-$PK_{cs}^{-/-}$* background induced synergistic sensitivity to IR. Transcriptome profiling using livers of *DNA-$PK_{cs}^{-/-}$* or *DNA-$PK_{cs}^{-/-}$RAD54$^{-/-}$* mice showed endogenous *CDKN1A* (p21) upregulation. In addition, *DNA-$PK_{cs}^{-/-}$* and *DNA-$PK_{cs}^{-/-}$RAD54$^{-/-}$* mice had increased and sustained p21 expression after IR treatment, compared to WT and *RAD54$^{-/-}$* mice. Moreover, DNA-PK_{cs} deficiency impaired dissolution of 53BP1, a marker for DSBs, in both mouse embryonic stem (mES) cells and mouse embryonic fibroblasts (MEFs). In this report we show evidence of mutually exclusive roles for HR and NHEJ in IR protection, where cell type or genetic background determines the extent of each pathway in which it partakes in DSB repair.

Keywords: Non-homologous end joining, DNA double strand break repair, DNA damage response, Ionizing radiation, Homologous recombination

INTRODUCTION

DNA double strand breaks (DSBs) constitute the most dangerous type of DNA damage induced by ionizing radiation (IR) (1). IR induced DNA damage can cause cell death or chromosomal instability, especially in cells with intrinsic DNA repair defects (2). In response to DNA damage, histones undergo posttranslational modifications including phosphorylation, acetylation, methylation and ubiquitination. Such histone modifications represent a histone code that directs the recruitment of protein involved in DNA damage sensing and repair processes (3,4). A long protein recruitment cascade starts with the recruitment of the E3 ubiquitin-protein ligase RNF8 (5). In turn, RNF8 starts an ubiquitination-cascade leading to RNF168-mediated mono-ubiquitination of lysine (K) 13-15 residues of histones of the H2A family (6). This ubiquitination-code can be recognized by a dimer of p53-binding protein 1 (53BP1) (7). The accumulation of 53BP1 at a lesion protects DNA ends from excessive 5' end-resection, thereby facilitating in DSB repair pathway choice (8). In addition, 53BP1 accumulation can be visualized as nuclear foci and can therefore be used as surrogate marker for DSBs.

All higher eukaryotes have at least two pathways of DSB repair, non-homologous end joining (NHEJ) and homologous recombination (HR). NHEJ operates throughout the cell cycle and is initiated by the Ku70/80 heterodimer, a ring shaped dimer which binds to DNA ends (9,10). Upon binding, DNA-PK_{CS} is recruited and activated by auto phosphorylation. At the final step, Ligase IV (LIG4) ligates processed DNA-ends (11,12). During the S and G2 phases of the cell cycle, HR is active as addition to NHEJ (13,14). The HR pathway starts with 5'-3' resection of the DNA ends, generating 3' single stranded DNA, stabilized by RPA (15,16). Recombination protein RAD51 then replaces RPA and forms a protein filament on the single stranded DNA, which facilitates the search for homology (17). RAD54 is a motor protein that increases the efficiency of homology search (18).

Although RAD54 binds directly to Rad51, its function is not essential and RAD54 mutant mice are viable, fertile and do not show IR sensitivity. Interestingly, in contrast to adult mice, *RAD54*$^{-/-}$ mouse embryos (E3.5) and mouse embryonic stem (mES) cells are IR sensitive (19,20). On the other hand, NHEJ deficient adult *scid* mice show IR sensitivity (20). Interestingly, *scid RAD54*$^{-/-}$ double mutant mice show higher IR sensitivity than the single mutants, a phenomenon which was also observed when deletions of KU80 or Lig4 are combined with the deletion of RAD54 (21,22). These observations led to the conclusion that HR and NHEJ function throughout development, in which HR possibly acts as a backup pathway for NHEJ in adult mice.

To further understand the cooperating role of NHEJ and HR we generated *RAD54*$^{-/-}$, *DNA-PK*$_{CS}^{-/-}$ and *DNA-PK*$_{CS}^{-/-}$*RAD54*$^{-/-}$ mutant mice. We report synergistic IR sensitivity when mice are disrupted in HR in a NHEJ deficient background. In addition, transcriptome analysis showed an elevated p21 stress response in *DNA-PK*$_{CS}^{-/-}$ and *DNA-PK*$_{CS}^{-/-}$*RAD54*$^{-/-}$ mutant mice which was increased and sustained after IR, compared to WT. Finally, we show that disrupting *DNA-PK*$_{CS}$ impairs 53BP1 foci dissolution and size increase in both MEFs and mES cells, while only

RAD54$^{-/-}$ mES cells showed similar phenotypes and *RAD54*$^{-/-}$ MEFs did not. Here we confirm both a primary and backup role for RAD54 in DSB repair in stem cells and differentiated cells, respectively. These results show that the role of either HR and NHEJ is mutually exclusive, depending on cell type or genetic background.

MATERIAL AND METHODS

Mice

All mice were backcrossed at least 8 times against C57/BL6, ensuring identical genetic background except for the mutations in *DNA-PK*$_{CS}$ and *RAD54*. To introduce the p21 reporter, *DNA-PK*$_{CS}$$^{-/-}$*RAD54*$^{-/-}$ mice were crossed with p21 reporter mice, a kind gift from the lab of Drs. Collin Henderson and Roland Wolf (23). All mice were kept under pathogen free conditions in individually ventilated cages in order to prevent infections.

Cell Culture

All Mouse Embryonic Fibroblast (MEFs), cell lines were cultured in Dulbecco's modified Eagle's medium (DMEM) mixed with Ham's F10 (1:1) supplemented with 1% Penicillin/Streptomycin and 10% Fetal Calf Serum (FCS). All mES cell lines were cultured DMEM in a 1:1 mixture with DMEM conditioned by exposure to a confluent monolayer of buffalo rat liver (BRL) cells in T175 flask, 50 mL FCS, 5 mL nonessential amino acids (Lonza), 200 U/mL penicillin, 200 µg/mL streptomycin, 89 µM β-mercaptoethanol, 1000 U/mL leukemia inhibitory factor. MEFs were incubated at 37 degrees in a water-saturated atmosphere with 5% CO_2 and 3% O_2. mES cells were incubated at 37 degrees in a water saturated atmosphere with 5% CO_2 and 20% O_2.

Irradiation

Mice survival experiments were performed by exposing the mice to 2 or 3 Gy using a 137-Cs source. Irradiation of p21-reporter mice was done using a microCT-imaging device (Quantum FX, Perkin Elmer). Radiation dosages relative to exposure time and magnification were previously determined (24). Irradiation was done with the following settings: 10 µm and 60 µm voxel size with 90 kV, 200 µA, and 3 min of scan time. By scanning the mice twice, the given dose was approximately 2 Gy.

All cells were irradiated using the RS320 (Xstrahl Live Sciences), a self-contained cabinet, with a dose rate of 1.6554 Gy/min (195 keV). Cells were cultured on round glass coverslips (diameter: 24 mm). To ensure a monolayer of mES cells the coverslips were coated with 0.05 mg/mL Laminin (Roche).

Clonogenic survival was performed as described before (19). In short, cells were seeded in the appropriate cell density and incubated for 7 hours. Subsequently, the cells were exposed to

2, 4 or 6 Gy of X-ray irradiation while control samples remained untreated. After 7 days colonies were counted manually.

Proliferation assays were performed based on the Sulforhodamine beta (SRB) assay. MEFs were seeded in 6-well plates (5×10^5 cells / well) and the next day adherent cells irradiated with 2, 4 or 6 Gy X-ray irradiation using the RS320, described above. Cells were trypsinized and seeded in triplicate in 12 well plates (1.5×10^4 cells per well) in 1 mL medium allowed to grow for one to six days. Subsequently, medium was removed and cells were fixed with 1 mL 10% trichloroacetic acid overnight at 4°C. Plates were washed five times with tap water and dried. Then cells were incubated in 500 µl 0.5% SRB in 1% acetic acid for 20 minutes at RT. Plates were washed four times with 1% acetic acid and air-dried. SRB was dissolved in 500 µl 10 mM Tris solution and absorbance was measured at 560 nm using a GloMax®-Multi Detection System (Promega).

Microarray analysis

Standard procedures were used to obtain total RNA (Qiagen) from the liver of 3-months old WT and DNA repair deficient mice. Synthesis of double stranded cDNA and biotin labeled cRNA was performed according to the instructions of the manufacturer (Affymetrix). Fragmented cRNA preparations were hybridized to full mouse genome oligonucleotide arrays (Affymetrix, mouse expression 430 V2.0 arrays), using a hybridization Oven 640 (Affymetrix), washed, and subsequently scanned on a GeneChip Scanner 3000 (Affymetrix). Initial data extraction and normalization within each array was performed by means of the GCOS software (Affymetrix). Data intensities were Log transformed and normalized within and between arrays by means of the quantile normalization method as previously described (25). Two-tailed pair wise analysis of variance was used by means of the Spotfire Decision Site software package 7.2 v10.0 (Spotfire Inc, Mass) to extract the statistically significant data from each of the 4 individual microarrays obtained for each genotype. The criteria for significance were set at $P\leq0.05$ and a positive or negative 1.2-fold change.

Gene Ontology classification and network analysis of all significant gene entries were subjected to GO classification (http://www.geneontology.org). Significant over-representation of GO-classified biological processes was assessed by comparing the number of pertinent genes in a given biological process to the total number of the relevant genes printed on the array for that particular biological process (Fisher exact test, $P\leq0.05$, False detection rate (FDR) ≤0.1) using the publicly accessible software Ease (26). Network analysis was performed through the use of Ingenuity Pathways Analysis, “a web-delivered application that enables biologists to discover, visualize and explore therapeutically relevant networks significant to their experimental results, such as gene expression array data sets (QIAGEN Inc, (27))”.

Quantitative RT-PCR

RT-PCR was performed as described before (28). In short, all reactions were run using the PerfeCTa® MultiPlex qPCR SuperMix (Quanta Biosciences, Inc., Gaithersburg, MD, USA), with primer and probe sets for target genes. Cycling parameters were 2 min at 95°C, then 45 cycles of 10 s at 95°C and 60 s at 60°C. Ct values were normalized to a HPRT1 internal control and converted to transcript quantity using standard curves.

Immunofluorescence

Fixed cells were washed with PBS and permeabilized using Triton buffer (0.1% Triton X-100 in PBS, 2x 10 min). Blocking was done for 30 minutes in PBS+ (0.5% BSA and 0.15% Glycin). Cells were incubated with primary antibody diluted in PBS+ for at least 2 hours at RT and washed with Triton buffer (2x 10 min) and PBS+ (1x short). Subsequently the cells were incubated with the secondary antibody for 1 hour in the dark. Primary antibodies used in this study are: 53BP1 (Novus Biologicals). Secondary antibodies used were conjugated to Alexa488 (Life Technologies).

Microscopy

To capture stained cells, a Leica SP5 confocal microscope was used. For each experiment 5 images were acquired using a 40x objective (NA = 1.25) and the appropriate laser lines and emission filters (DAPI/Atto Azide 390; ex. 405 nm – em. 435-480, Alexa 488; ex. 488 nm – em. 500-550 nm, Alexa 594; ex. 561 nm – em. 570-630 nm). For image analysis, z-projections were made and cell nuclei were analysed for 53BP1 foci number and area using homemade ImageJ scripts. In short, cell nuclei were segmented using the DAPI signal by auto-thresholds. Within the segmented nuclei, segmentation masks were made for individual foci using auto-thresholds and the watershed tool (29). The mean area and number of the segmented foci were measured via the measure option of ImageJ.

RESULTS

DNA-PK$_{CS}$ and RAD54 mutations have synergistic effect on IR sensitivity

To investigate the interplay between HR and NHEJ dependent DSB repair, we chose for an experimental set up in which we could detect possible differences between Wild-Type (WT) mice with deficiencies in non-essential gene involved in NHEJ and HR. DSB repair deficiency was achieved either by deletion of *DNA-PK*$_{CS}$ (NHEJ) or *RAD54* (HR). To analyze the consequences of combined NHEJ and HR deficiency, we used mice where both genes were disrupted.

We previously found that while *RAD54*$^{-/-}$ mice were not IR hypersensitive, *DNA-PK* mutant mice (*scid*) which were in addition *RAD54* deficient were hypersensitive to IR compared to single *scid* mice (20). Therefore, we first analyzed the IR sensitivity of single *DNA-PK*$_{CS}$$^{-/-}$ and

double DNA-$PK_{CS}^{-/-}$ $RAD54^{-/-}$ mutant mice. While all *DNA-*$PK_{CS}^{-/-}$ single mutant mice survived a single exposure to 2 Gy, all *DNA-*$PK_{CS}^{-/-}$*RAD54*$^{-/-}$ mice died after irradiation with 2 Gy γ-radiation, within a period of 13 days (Figure 1A). A single exposure to 3 Gy of γ-radiation resulted in earlier death of all *DNA-*$PK_{CS}^{-/-}$*RAD54*$^{-/-}$ mice compared to *DNA-*$PK_{CS}^{-/-}$ mice of which 50% did not survive the treatment after 16 days (Figure 1B).

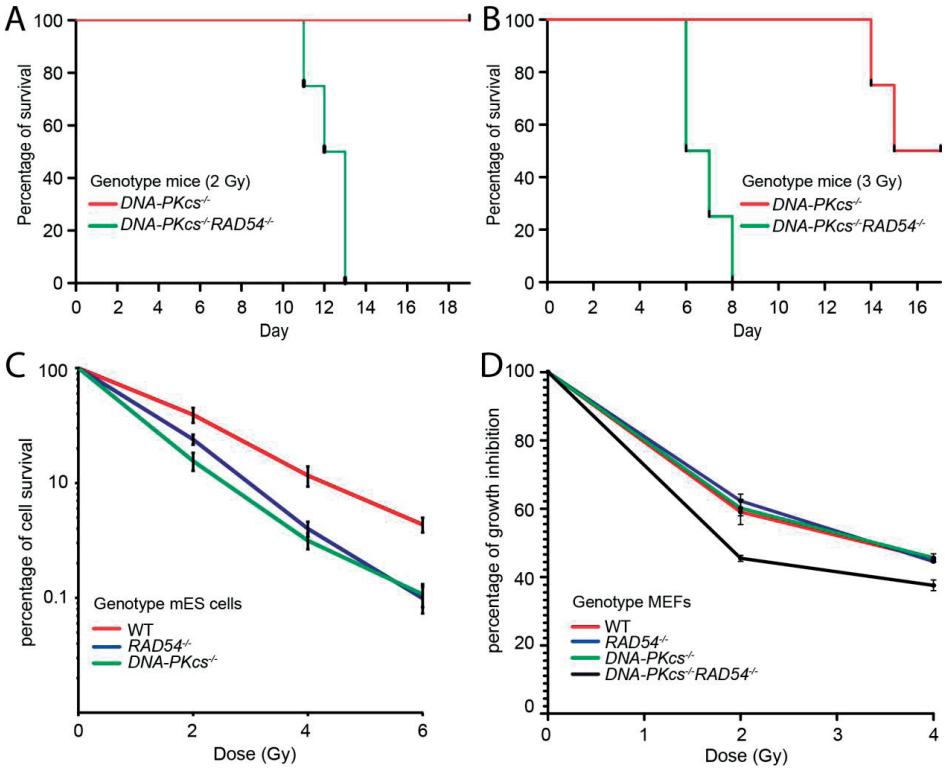

Figure 1. *DNA-*PK_{CS} and *RAD54* mutations have synergistic effect on IR sensitivity in mice.
DNA-$PK_{CS}^{-/-}$ and DNA-$PK_{CS}^{-/-}$RAD54$^{-/-}$ mice were irradiated with 2 **(A)** or 3 **(B)** Gy and tested for survival. The curves represent 5 mice per group. Red and green are represented by indicated genotypes. **(C)** Clonogenic survival of mES cells with indicated genotypes. **(D)** Proliferation assay (SRB) of MEFs with indicated genotypes. Cells were irradiated and grown for 6 days, the SRB assay measures the amount of protein present after 6 days in culture.

To investigate the IR sensitivity of embryonic cells we compared mES cells with either disrupted *RAD54* or *DNA-*PK_{CS}. We observed a 2.5 fold increased IR sensitivity both in *RAD54*$^{-/-}$ and *DNA-*$PK_{CS}^{-/-}$ mES cells compared to WT (Figure 1C). Differentiation of human induced pluripotent or ES cells decreases DNA damage repair by HR (30). We wanted to analyze whether this phenomenon could explain the difference in IR sensitivity between *RAD54* deficient mES cells and *RAD54* deficient adult mice. Using isolated mouse embryonic fibroblasts (MEFs) we performed

proliferation assays to assess the IR sensitivity of differentiated cells deficient in *RAD54*, *DNA-PK$_{CS}$* or both. We found that *DNA-PK$_{CS}^{-/-}$RAD54$^{-/-}$* MEFs show growth inhibition compared to all other genotypes (Figure 1D). IR sensitivity of fibroblasts in this proliferation assay was found in MEFs isolated from *DNA-PK$_{CS}^{-/-}$RAD54$^{-/-}$* adult mice, which showed the highest IR sensitivity in overall survival. We conclude that both HR and NHEJ contribute to IR protection in mES cells. In addition, IR sensitivity of MEFs and adult mice is only observed by deletion of both HR in a NHEJ deficient background, suggesting that HR switches from main DSB repair pathway in mES cells to a back-up role in differentiated cell types.

CDKN1A is upregulated in *DNA-PK$_{CS}$* and *DNA-PK$_{CS}$RAD54* deficient mice

We compared the transcriptional responses in untreated WT and DSB deficient mice to analyze whether and which molecular processes are differentially affected in untreated DSB repair deficient animals. To this end, mRNA expression levels were determined in the liver of three months old WT and DNA repair deficient mice. We selected genes that were significantly differentially expressed between WT and DNA repair deficient mice. We found 589 probe sets, which showed a more than 1.2-fold change in gene expression at a FDR of 0.05, yielding 246 unique probes that were used for further molecular pathways discovery analysis in Ingenuity Pathway Analysis (IPA).

IPA network analysis showed that one of the most extensively affected genetic networks in livers of *DNA-PK$_{CS}^{-/-}$RAD54$^{-/-}$* mice was centered on the *CDKN1A* gene (Figure S1). The *CDKN1A* gene encodes for the p21 protein, a p53-regulated DNA damage response gene (31). Comparing this network to both *DNA-PK$_{CS}^{-/-}$* and *RAD54$^{-/-}$* mice showed upregulation of *CDKN1A* in livers of *DNA-PK$_{CS}^{-/-}$* mice but not in livers of *RAD54$^{-/-}$* mice (Figures S2 and S3). *CDKN1A* was significantly upregulated in *DNA-PK$_{CS}^{-/-}$* and *DNA-PK$_{CS}^{-/-}$RAD54$^{-/-}$* livers, with higher levels of expression in *DNA-PK$_{CS}^{-/-}$RAD54$^{-/-}$* compared to *DNA-PK$_{CS}^{-/-}$* mice (Supplemental table 1). We conclude that inactivation of DNA-PK$_{CS}$ leads to upregulation of p21 in the liver. Although deletion of RAD54 alone did not lead to p21 upregulation in the liver, the deletion of RAD54 in a *DNA-PK$_{CS}^{-/-}$* background did lead to increased upregulation of p21 (Figure 2A).

To confirm these results we performed quantitative reverse transcription PCR (RT-qPCR) cDNA, generated from isolated RNA that was used for previous mRNA expression analysis. We found similar results as the mRNA expression analysis; deletion of DNA-PKcs alone led to upregulation of p21 expression while deleting RAD54 alone did not, unless RAD54 was deleted in a *DNA-PK$_{CS}^{-/-}$* background (Figure 2B). We conclude that the DNA damage response was upregulated in the livers of *DNA-PK$_{CS}^{-/-}$* mice compared to WT and *RAD54$^{-/-}$* mice possibly due to the deficiency in the ability to repair endogenous DNA damage. Even the very low levels of endogenous DSBs in unirradiated conditions are sufficient to activate the p21 response, suggesting that this may be a highly sensitive marker for DNA damage.

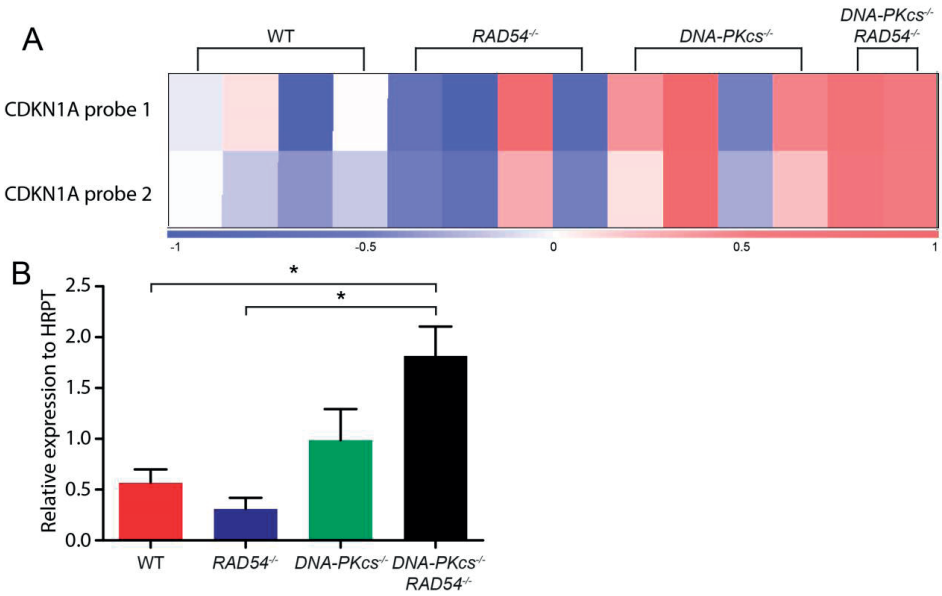

Figure 2. ***CDKN1A* is upregulated in *DNA-PK$_{cs}$* and *DNA-PK$_{cs}$RAD54* deficient mice. (A)** OmniViz heatmap showing the differential expression of CDKN1A, measured with two different probes, between indicated genotypes in untreated mice livers. Gene expression levels: red, upregulated genes compared to the geometric mean; blue, downregulated genes compared to the geometric mean. Color intensity correlated with the degree of change. **(B)** Quantitative RT-PCR analysis of gene expression in untreated mice livers of indicated genotypes. Values were normalized using *HPRT* as standard. The mean values represent at least three mice of similar genotypes (error bars express the SE).

CDKN1A expression as readout for IR sensitivity in DNA repair mutant mice

Since we found expression of the *CDKN1A* gene upregulated in DSB DNA repair deficient mice, we subsequently wanted to evaluate *CDKN1A* expression levels *in vivo* in mice of various repair deficient backgrounds using *CDKN1A*-luciferase reporter mice (23). The reporter construct was directed to the end of exon 3 of the endogenous p21 locus where a sequence, which encodes for T2A-β-gal-T2A-luciferase, was inserted. This insertion led expression of p21, β-gal and luciferase from the one engineered allele. DSB DNA repair deficient mice were crossed with *CDKN1A*-luciferase reporter mice, which led to both hetero- and homozygous animals for the reporter loci. For further experiments, we selected DSB DNA repair animals that were homozygous for the p21 reporter loci. As a control for background luminescence, we used WT mice without any reporter loci, which showed no bioluminescent signal upon injection of luciferin. Consistent with the previous finding, we observed increased endogenous p21-luciferase expression in both untreated *DNA-PK$_{cs}^{-/-}$* and *DNA-PK$_{cs}^{-/-}$RAD54$^{-/-}$* mice compared to WT and *RAD54$^{-/-}$* mice (Figure 3A).

It has been shown that exposing p21-reporter mice to different doses of IR, *in vivo* DNA damage induction can be monitored, non-invasively and dose-dependent, using luciferase as marker

for p21 expression (23). To evaluate DNA damage induced by IR, DNA DSB repair deficient mice expressing the p21-reporter construct were irradiated with a single dose of 2 Gy. For both wild type and *RAD54*$^{-/-}$ mutant mice, the p21 expression increased within 4 hours after irradiation and returned to background levels 24 hours after irradiation (Figure 3A). Interestingly, for both *DNA-PK*$_{CS}$$^{-/-}$ and *DNA-PK*$_{CS}$$^{-/-}$*RAD54*$^{-/-}$ mutant mice the p21 expression was higher at 4 hours after irradiation, compared to WT and *RAD54*$^{-/-}$. In addition, p21 expression did not decline after 24 hours in *DNA-PK*$_{CS}$$^{-/-}$ and *DNA-PK*$_{CS}$$^{-/-}$*RAD54*$^{-/-}$ mutant mice.

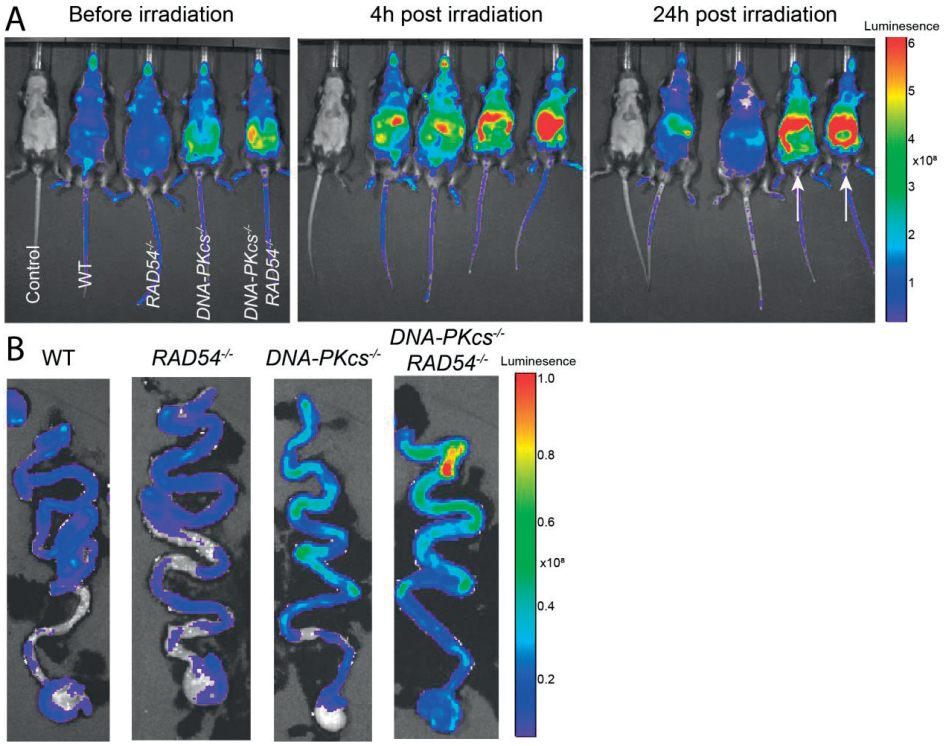

Figure 3. *CDKN1A* expression as readout for radio sensitivity in DNA repair mutant mice.
Bioluminescent imaging of p21-reporter mice crossed with indicated genotypes. **(A)** Mice were irradiated using µCT imaging and were imaged for bioluminescent signal before irradiation, 4 hours post irradiation, and 24 hours post irradiation. Genotype order was the same for every time-point. **(B)** Ex-vivo images of the small intestine 24 hours after irradiation.

Tissue absorbance of bioluminescent signal is a limiting factor for deep-tissue imaging using this technique. Therefore, the observed bioluminescent signal probably originates from organs directly under the skin, such as the intestinal tract. Indeed, ex vivo scanning showed high luciferase expression in *DNA-PK*$_{CS}$$^{-/-}$ and *DNA-PK*$_{CS}$$^{-/-}$*RAD54*$^{-/-}$ mutant intestinal tracts after 24 hours, similar as the whole body scans (Figure 3B). We conclude that mice lacking DNA-PK$_{CS}$ or RAD54 and DNA-PK$_{CS}$ show increased expression of p21 in untreated conditions and sustained expres-

sion after IR, consistent with our previous finding of p21 upregulation in livers of *DNA-PK$_{CS}^{-/-}$* and *DNA-PK$_{CS}^{-/-}$RAD54$^{-/-}$* mice. In addition, p21 expression in *DNA-PK$_{CS}^{-/-}$* and *DNA-PK$_{CS}^{-/-}$RAD54$^{-/-}$* mice is high in the intestinal tract and does not decline after 24 hours, probably due to residual DNA damage.

Impaired 53BP1 foci disappearance in MEFs cells lacking *DNA-PK$_{CS}$*

The upregulated and sustained p21-mediated stress response in *DNA-PK$_{CS}^{-/-}$ and DNA-PK$_{CS}^{-/-}$ RAD54$^{-/-}$* mice is most likely directly related to the IR sensitivity and the hypersensitivity of the respective genotypes. We speculated that the DNA might contain increased levels of spontaneous or residual DSBs. In order to investigate this directly, we analyzed MEFs of the four genotypes and for three genotypes of mES cells, for their endogenous 53BP1 foci and IR induced foci.

MEFs were analyzed for the number of 53BP1 foci in untreated conditions and 2, 6, 18, 30, and 72 hours after IR. We observed that the number of 53BP1 foci increased after IR and decreased over time in both WT and *RAD54$^{-/-}$* cells. Interestingly, the number of 53BP1 foci decreased much more slowly in MEFs lacking DNA-PK$_{CS}$ than WT and *RAD54$^{-/-}$* MEFs (Figure 4A).

In order to quantify the number of foci, we used automated ImageJ scripts to process confocal images and analyze 53BP1 foci per µm^2 of the nucleus. We found no significant differences in the endogenous number of 53BP1 foci between the four genotypes. Treatment with IR increased the number of 53BP1 foci in WT and *RAD54$^{-/-}$* MEFs, which after 72 hours reached similar number of 53BP1 foci as the endogenous condition. However, the course of IR induced number of 53BP1 foci was drastically different when DNA-PK$_{CS}$ was disrupted (Figure 5A). In both *DNA-PK$_{CS}^{-/-}$* and *DNA-PK$_{CS}^{-/-}$RAD54$^{-/-}$* MEFs, the IR induced number of 53BP1 foci was significantly higher compared to other genotypes. In addition, in *DNA-PK$_{CS}^{-/-}$* and *DNA-PK$_{CS}^{-/-}$ RAD54$^{-/-}$* MEFs the number of 53BP1 foci did not decrease to their respective endogenous levels after 72 hours. These results correlate with the observation of the sustained p21 expression after IR in both *DNA-PK$_{CS}^{-/-}$* and *DNA-PK$_{CS}^{-/-}$RAD54$^{-/-}$* adult mice.

In addition, mES cells were analyzed for the number of 53BP1 foci in untreated conditions and 2, 6, 8, 18 and 24 hours after IR. We observed that the number of 53BP1 foci increased after IR and decreased over time in WT cells. Interestingly, the number of 53BP1 foci decreased with slower kinetics in mES cells lacking RAD54 or DNA-PK$_{CS}$ than in WT cells (Figure 4B).

Again, the number of 53BP1 foci was quantitatively analyzed per µm^2 of the nucleus. Similar as the MEFs, we found no significant difference in the endogenous number of 53BP1 foci for all three genotypes. IR treatment of WT mES cells showed an increase in the number of 53BP1 foci, which returned to similar numbers as untreated conditions after 24 hours (Figure 5B). *DNA-PK$_{CS}^{-/-}$* mES cells showed less initial 53BP1 foci after IR compared to both WT and *RAD54$^{-/-}$* mES cells. *RAD54$^{-/-}$* mES cells also show a delayed reduction of 53BP1 foci, compared to WT cells. We conclude that both DNA-PK$_{CS}$ and RAD54 have a role in the reducing the number of 53BP1

foci in mES cells, while DNA-PK_{CS} showed to have this role in MEFs and not RAD54. In addition, as deduced from 53BP1 foci kinetics in mES cells, RAD54 deficiency alone already affected DSB repair, which correlates with the suggestion of a larger role of HR in undifferentiated cells (30).

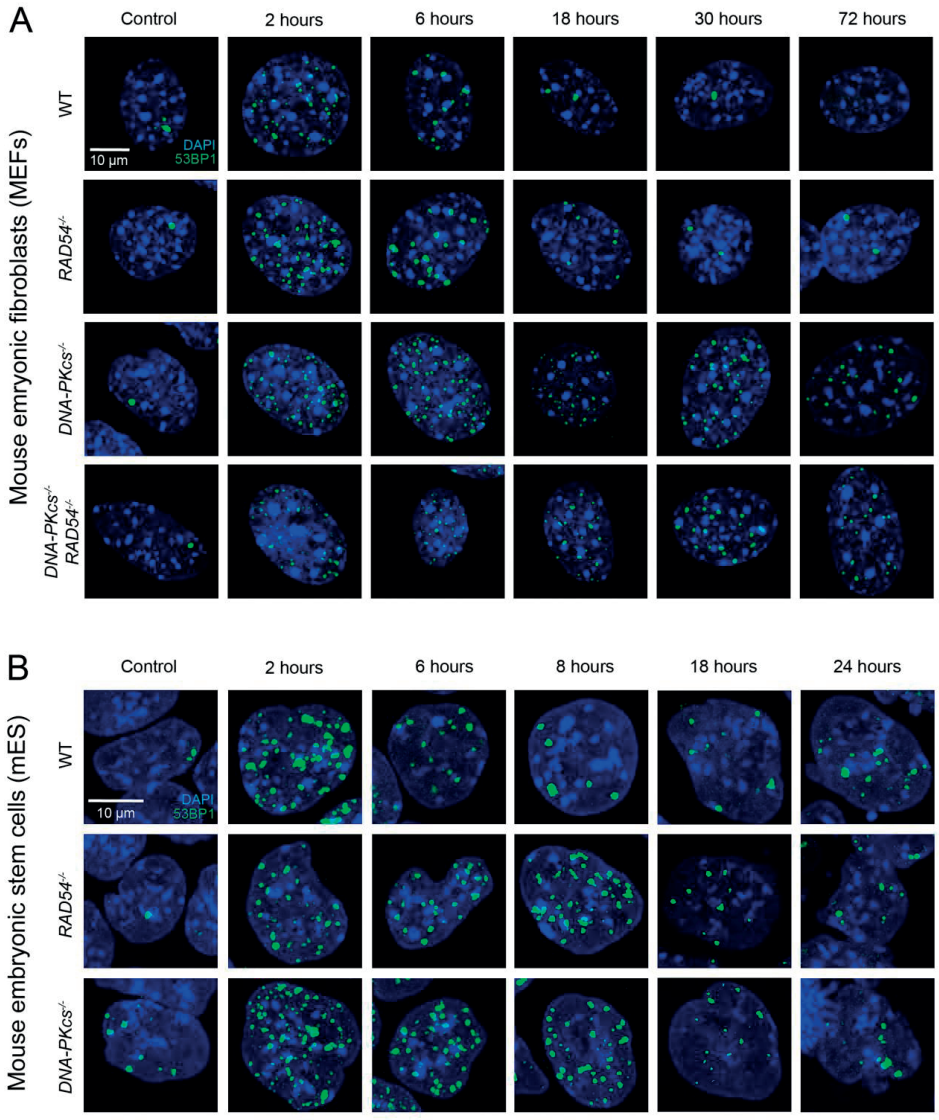

Figure 4. Overview of MEFs and mES cells 53BP1 foci disappearance over time.
MEFs and mES were irradiated with 2 Gy X-ray irradiation and incubated to recover for indicated time. Cells were stained for endogenous 53BP1 (green) and DAPI (blue). Scale bar indicates 10 µm.

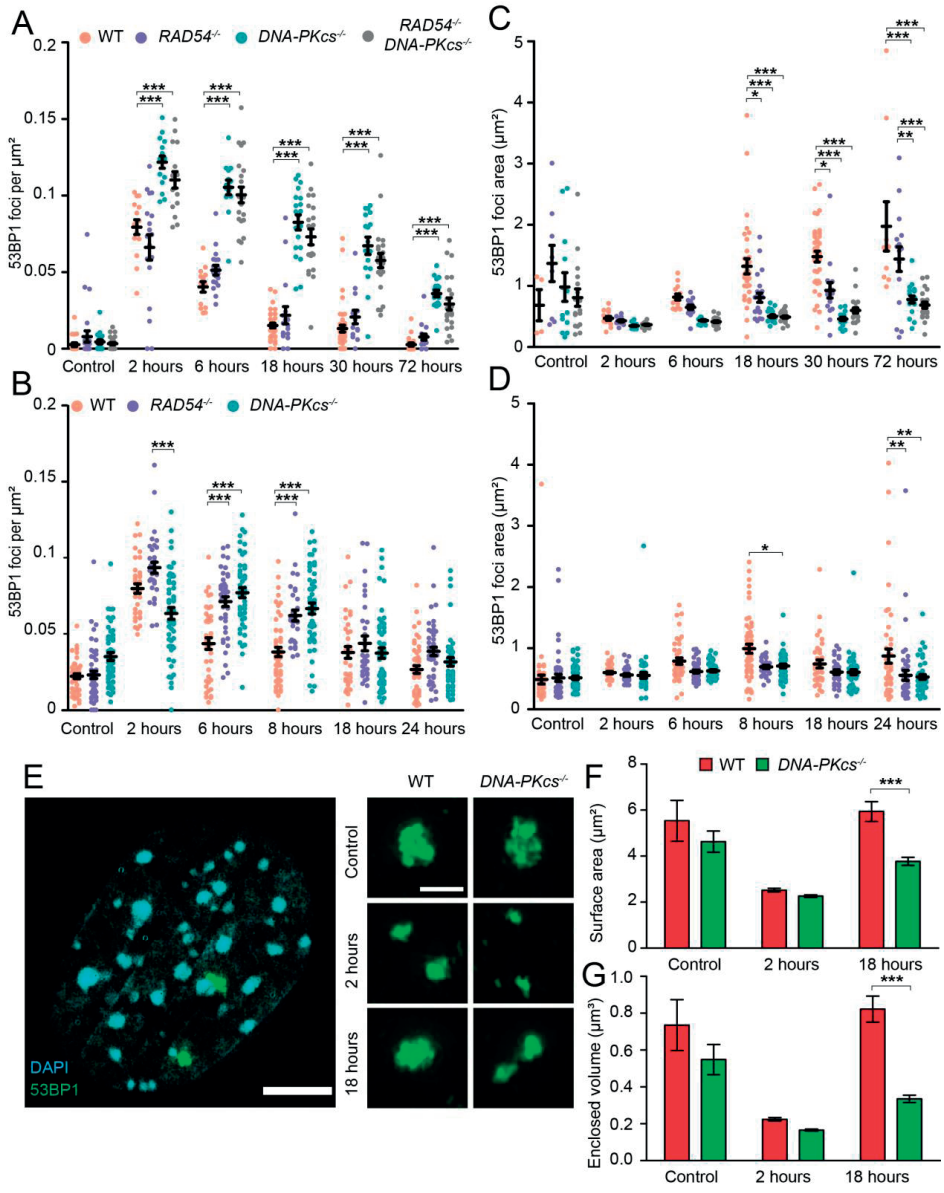

Figure 5. Impaired 53BP1 foci disappearance in MEFs and mES cells deficient for *DNA-PK$_{cs}$*.
Quantification of 53BP1 foci per µm^2 MEF nuclei (A) and average 53BP1 focus size (C). Quantification of 53BP foci per µm^2 mES nuclei (B) and average 53BP1 focus size (D). Per assay >50 nuclei were analyzed. Error bars indicate SEM. (E) SIM image of a WT MEF stained for 53BP1 (green) and DAPI (blue), including representative images of 53BP1 foci in WT and DNA-PK$_{CS}^{-/-}$ MEFs at control conditions, 2 and 18 hours after irradiation. Scale bars represent 5 µm on the left and 0.5 µm on the right. (F) Quantification of the surface area of 53BP1 in 3D. (G) Quantification of the enclosed volume of 53BP1 in 3D. For the quantification >100 53BP1 foci were analyzed. Error bars indicate SEM.

53BP1 foci growth is delayed or absent in DNA repair deficient MEFs and mES cells

Whilst investigating foci disappearance, we noticed that the size of 53BP1 foci was increased at later time points and was different between genotypes (Figure 4A and B). We used automated ImageJ scripts to process confocal images and quantitatively analyzed differences in 53BP1 foci size (μm^2) at the same time points as we analyzed the number of 53BP1 foci. In MEFs, the size of 53BP1 foci in unirradiated conditions showed no significant difference between the genotypes. Interestingly, IR decreased the size of 53BP1 foci for all genotypes, following by an increase over time which was only observed in WT and, to a lesser extent, in *RAD54*$^{-/-}$ MEFs (Figure 5C). MEFs lacking DNA-PK$_{CS}$ did not show any significant increase of 53BP1 foci size up to 72 hours.

Presented confocal images were analyzed by using maximal projections, not harboring possible information in the z-direction. Structured Illumination Microscopy (SIM) is a super-resolution technique which has a higher resolution. By comparing 3D structures of 53BP1 foci in WT and *DNA-PK$_{CS}$*$^{-/-}$ MEFs we observed decrease of size after IR and the absence of size increase in *DNA-PK$_{CS}$*$^{-/-}$ MEFs (Figure 5E). In order to analyze the shape of these structures more quantitatively, we calculated the surface area and enclosed volume of the 3D objects. Both the surface area and enclosed volume of 53BP1 foci decreased after irradiation (Figure 5F and G). In addition, both values reached control values in WT MEFs while in *DNA-PK$_{CS}$*$^{-/-}$ MEFs it did not.

The increase of 53BP1 foci size showed a different course in mES cells. We observed a slight increase in size in WT mES cells within 24 hours (Figure 5D). Both *RAD54*$^{-/-}$ and *DNA-PK$_{CS}$*$^{-/-}$ mES cells showed no significant difference in 53BP1 foci size increase until 24 hours post IR, compared to WT.

DISCUSSION

We explored the roles of HR and NHEJ in IR protection by combining HR mutant (RAD54-/-) with NHEJ mutant (DNA-PKCS-/-) mice and cells. We found that the p21 stress response was endogenously elevated in the liver tissue of DNA-PKCS-/- mice and even higher in DNA-PKCS-/-RAD54-/- mice. Moreover, after IR, the p21 stress response in both DNA-PKCS-/- and DNA-PKCS-/-RAD54-/- mice was hyper activated and sustained. We showed that 53BP1 foci dissolution and growth in both MEFs and mES cells lacking DNA-PKCS was impaired. These findings indicate that a combination of NHEJ and HR, in which the extent of each pathway is dependent cell type or genetic background, controls IR protection.

Prominent role of HR as back-up DNA damage repair mechanism in differentiated cells and adult mice

The IR hypersensitivity of *DNA-PK$_{CS}$*$^{-/-}$*RAD54*$^{-/-}$ mice compared to *DNA-PK$_{CS}$*$^{-/-}$ mice phenocopies the synergistic effect of a combined *RAD54* mutation with the *scid* mutation. The *scid* mice

are homozygous for a defect in the mouse homologue of the human *PRKDC*-gene, which leads to an inactive DNA-PK_{CS} protein (32). Thus, the inactivation of DNA-PK_{CS} as in *scid* mice leads to similar IR sensitivity compared to *DNA-PK_{CS}-/-* mice. Interestingly, the phenotype of single mutant *DNA-PK_{CS}* mice is much milder compared to the inactivation of KU80 or LIG4. The loss of KU80 leads to small animal sizes and early death, while loss of LIG4 results in late embryonic death (20-22). In addition, disrupting either KU80 or LIG4 in combination with RAD54 has been reported to cause large amounts of endogenous yH2AX foci (21,22). Interestingly, we did not observe endogenous differences between WT or mutant MEFs and mES cells in number of 53BP1 foci. The absence of endogenous foci in *DNA-$PK_{CS}^{-/-}$RAD54$^{-/-}$* MEFs could implicate a partial role of DNA-PK_{CS} in repair of DSBs arising in S/G2-phase in which KU80 and LIG4 have larger roles. Indeed, DNA-PK_{CS} is reported to be relatively dispensable in the ligation of blunt signal ends in V(D)J recombination (33). Moreover, KU80 has a role in DNA-end protection and LIG4 in ligation of DNA-ends, while DNA-PK_{CS} has been described to have a more 'facilitating' role, mostly tethering NHEJ factors for increased efficiency (34). Apparently, tethering of NHEJ factors is not crucial in the repair of endogenous DNA damage, revealing a less severe effects of DNA-PK_{CS} loss.

Although we did not observe endogenous elevated DNA damage levels between mutant cells, we found differences in IR sensitivity between mutant MEFs and mES cells. We observed that *DNA-$PK_{CS}^{-/-}$RAD54$^{-/-}$* MEFs showed increased IR sensitivity compared to other genotypes. This finding could be compared with the hyper sensitivity of adult mice, suggesting that introducing HR deficiency in a NHEJ deficient background eliminates the back-up role of HR. Taken together, these reports and the observations in this work are suggesting a that HR functions as a back-up DNA damage repair mechanism in differentiated cells and adult mice.

Role for DNA-PK_{CS} in 53BP1 foci induction and dissolution during DNA DSB repair

Disrupted DNA-PK_{CS} leads to more foci per cell after 2 hours, compared to all other genotypes, and impaired dissolution in both MEFs and mES cells. Both *DNA-$PK_{CS}^{-/-}$* and *DNA-$PK_{CS}^{-/-}$RAD54$^{-/-}$* MEFs showed a 2-fold higher induction of initial 53BP1 foci and had not reached similar number of 53BP1 foci as control after 72 hours, while *RAD54$^{-/-}$* MEFs was comparable with WT. The many emerging studies examining the kinetics of DSB repair provided insightful information on DSB repair pathway use (35). For example, it was reported that in the G2-phase of the cell cycle the fast NHEJ pathway repairs 70% of IR-induced DSB. In addition, in G1 up to 80% of the DSBs is thought to be repaired by NHEJ (34). Although Ku has a crucial function as protection of DNA-ends (36), the assembly of the DNA-PK complex ensures tethering of other NHEJ factors. The tethering of NHEJ core-protein is dependent on the kinase activity of DNA-PK_{CS} and thought to contribute to efficient DSB repair by NHEJ (37,38). Therefore, the depletion of DNA-PK_{CS} could decrease the efficiency of NHEJ, making the depletion of DNA-PK_{CS} not as impactful as depletion of Ku (39). The impaired efficiency of NHEJ by DNA-PK_{CS} depletion could explain the impaired 53BP1 foci resolving of *DNA-$PK_{CS}^{-/-}$* and *DNA-$PK_{CS}^{-/-}$RAD54$^{-/-}$* MEFs and *DNA-$PK_{CS}^{-/-}$* ES cells.

Additionally, 53BP1 foci growth in both *DNA-PK$_{CS}^{-/-}$* and *DNA-PK$_{CS}^{-/-}$RAD54$^{-/-}$* MEFs was significantly impaired compared to *RAD54$^{-/-}$* and WT MEFs. DSB foci growth is caused by chromatin decondensation or expansion of chromatin signaling (34). ATM initiates the IR-induced chromatin signaling cascade to phosphorylate H2AX. However, in ATM-deficient cells phosphorylation of H2AX still occurs mediated by DNA-PK$_{CS}$ (40). In addition, ATM also has an important role in phosphorylating KAP1, driving local chromatin decondensation as result of ionizing radiation exposure. Interestingly, both phosphorylation of KAP1 and chromatin decondensation was diminished in *DNA-PK$_{CS}^{-/-}$* HCT116 cells, while ATM inhibition had no additional effect (41-43). These reports suggest an active role for DNA-PK$_{CS}$ in the initial amplification of chromatin signaling and decondenstation. Recruitment of 53BP1 is a consequence of H2AX phosphorylation, mediated by the RNF8 ubiquitination cascade, and could therefore be impaired in a *DNA-PK$_{CS}^{-/-}$* background (44). Collectively, the impaired 53BP1 foci growth in *DNA-PK$_{CS}^{-/-}$* cell lines could be the cause of inefficient ATM-dependent chromatin signaling or KAP1-dependent chromatin decondensation.

Analysis of the p21 response in DNA DSB repair deficient mice

The p53 tumor suppressor protein mediates the transcriptional regulation of p21. Hence, in response of DNA damage, p21 expression is upregulated. The p21 protein has a central role in determining cellular responses to cellular results, mainly by inhibitory control over the cell cycle (31). We investigated the *in vivo* p21 expression following IR using p21-reporter mice, which showed endogenous elevated p21 expression in mice lacking DNA-PK$_{CS}$. Moreover, we found that p21 expression was hyper activated and sustained after IR in *DNA-PK$_{CS}^{-/-}$* and *DNA-PK$_{CS}^{-/-}$RAD54$^{-/-}$* mice, mainly in the highly proliferative intestinal tract. This correlates with the observation of impaired 53BP1 dissolution in *DNA-PK$_{CS}^{-/-}$* MEFs and mES. Interestingly, the introduction of RAD54 mutations had no additive effect on the impaired DSB repair in *DNA-PK$_{CS}^{-/-}$* MEFs. This seems contradictory to adult mice, where RAD54 deletion was synergistic for IR resistance and induced higher p21 expression. A possible reason could be that the role of RAD54 in genome maintenance is differential between tissues. Consistent with this, we found that RAD54 depletion in mES cells did cause impaired 53BP1 foci resolving, which could be extrapolated to the IR sensitivity of *RAD54$^{-/-}$* embryo's (20).

It is interesting to speculate that IR protection is differentially regulated between tissues. An abundance of work has been documented on how high-dose IR affects mice, which showed that the gastrointestinal (GI) system is the most affected, leading to the survival of 6-8 days (45). We observed a maximum of 8 days of survival after 3 Gy in an *DNA-PK$_{CS}^{-/-}$RAD54$^{-/-}$* background (Figure 1). In addition, the combination of KU80 and RAD54 deficiency showed similar survival after 0.2 Gy (21). Moreover, IR induced sustained p21 expression in the GI of *DNA-PK$_{CS}^{-/-}$* and *DNA-PK$_{CS}^{-/-}$RAD54$^{-/-}$*, suggesting unrepaired DNA damage (Figure 3B).

Together with our finding that RAD54 might have a larger role in embryonic cells compared to differentiated cells in DSB repair, suggest that the embryonic crypt villi in the GI have a limiting

role in IR protection. This would explain the synergistic effect of *RAD54* depletion in adult mice in a NHEJ background, making embryonic cells in the GI highly sensitive for IR.

In conclusion, we demonstrate that the p21 response is a highly sensitive DNA damage marker, able to detect endogenous DNA damage in mice deficient for NHEJ. In differentiated cells, only NHEJ is required for efficient 53BP1 foci dissolution and growth, while in stem cells both NHEJ and HR are required. Our data are consistent with a prominent role for HR in undifferentiated cell types, switching to the background during differentiation of cells. Together, our findings suggest that cell type or genetic background determines the extent of which NHEJ or HR partakes in repair of IR induced DSBs

ACKNOWLEDGEMENTS

We would like to thank Dr. F. Alt for the *DNA-PKCS-/-* mES cell lines, Dr. G. Taccioli for *DNA-PKCS* deficient mice. In addition, we would like to thanks Stijn de Jong for his contribution on quantifying 53BP1 foci. This work was supported with imaging equipment provided by the Applied Molecular Imaging Erasmus MC facility (AMIE). This project was funded by Technologie stichting STW, project number 13577.

REFERENCES

1. Shibata, A. and Jeggo, P.A. (2014) DNA double-strand break repair in a cellular context. *Clin Oncol (R Coll Radiol)*, **26**, 243-249.
2. Hoeijmakers, J.H. (2009) DNA damage, aging, and cancer. *N Engl J Med*, **361**, 1475-1485.
3. Jackson, S.P. and Bartek, J. (2009) The DNA-damage response in human biology and disease. *Nature*, **461**, 1071-1078.
4. Panier, S., Ichijima, Y., Fradet-Turcotte, A., Leung, C.C.Y., Kaustov, L., Arrowsmith, C.H. and Durocher, D. (2012) Tandem Protein Interaction Modules Organize the Ubiquitin-Dependent Response to DNA Double-Strand Breaks. *Molecular Cell*, **47**, 383-395.
5. Huen, M.S.Y., Grant, R., Manke, I., Minn, K., Yu, X., Yaffe, M.B. and Chen, J. (2007) RNF8 Transduces the DNA-Damage Signal via Histone Ubiquitylation and Checkpoint Protein Assembly. *Cell*, **131**, 901-914.
6. Mattiroli, F., Vissers, J.H., van Dijk, W.J., Ikpa, P., Citterio, E., Vermeulen, W., Marteijn, J.A. and Sixma, T.K. (2012) RNF168 ubiquitinates K13-15 on H2A/H2AX to drive DNA damage signaling. *Cell*, **150**, 1182-1195.
7. Panier, S. and Boulton, S.J. (2014) Double-strand break repair: 53BP1 comes into focus. *Nat Rev Mol Cell Bio*, **15**, 7-18.
8. Ochs, F., Somyajit, K., Altmeyer, M., Rask, M.B., Lukas, J. and Lukas, C. (2016) 53BP1 fosters fidelity of homology-directed DNA repair. *Nature Structural and Molecular Biology*, **23**, 714-721.
9. Gottlieb, T.M. and Jackson, S.P. (1993) The DNA-Dependent Protein-Kinase - Requirement for DNA Ends and Association with Ku Antigen. *Cell*, **72**, 131-142.
10. Ciccia, A. and Elledge, S.J. (2010) The DNA Damage Response: Making It Safe to Play with Knives. *Molecular Cell*, **40**, 179-204.
11. Yannone, S.M., Khan, I.S., Zhou, R.Z., Zhou, T., Valerie, K. and Povirk, L.F. (2008) Coordinate 5' and 3' endonucleolytic trimming of terminally blocked blunt DNA double-strand break ends by Artemis nuclease and DNA-dependent protein kinase. *Nucleic Acids Res*, **36**, 3354-3365.
12. Ahnesorg, P., Smith, P. and Jackson, S.P. (2006) XLF interacts with the XRCC4-DNA ligase IV complex to promote DNA nonhomologous end-joining. *Cell*, **124**, 301-313.
13. Lieber, M.R. (2010) The mechanism of double-strand DNA break repair by the nonhomologous DNA end-joining pathway. *Annu Rev Biochem*, **79**, 181-211.
14. Wyman, C. and Kanaar, R. (2006) DNA Double-Strand Break Repair: All's Well that Ends Well. *Annual Review of Genetics*, **40**, 363-383.
15. Densham, R.M. and Morris, J.R. (2019) Moving Mountains-The BRCA1 Promotion of DNA Resection. *Front Mol Biosci*, **6**, 79.
16. Chen, H., Lisby, M. and Symington, L.S. (2013) RPA coordinates DNA end resection and prevents formation of DNA hairpins. *Mol Cell*, **50**, 589-600.
17. Liu, J., Doty, T., Gibson, B. and Heyer, W.D. (2010) Human BRCA2 protein promotes RAD51 filament formation on RPA-covered single-stranded DNA. *Nat Struct Mol Biol*, **17**, 1260-1262.
18. Renkawitz, J., Lademann, C.A., Kalocsay, M. and Jentsch, S. (2013) Monitoring homology search during DNA double-strand break repair in vivo. *Mol Cell*, **50**, 261-272.
19. Essers, J., Hendriks, R.W., Swagemakers, S.M., Troelstra, C., de Wit, J., Bootsma, D., Hoeijmakers, J.H. and Kanaar, R. (1997) Disruption of mouse RAD54 reduces ionizing radiation resistance and homologous recombination. *Cell*, **89**, 195-204.

20. Essers, J., van Steeg, H., de Wit, J., Swagemakers, S.M., Vermeij, M., Hoeijmakers, J.H. and Kanaar, R. (2000) Homologous and non-homologous recombination differentially affect DNA damage repair in mice. *EMBO J*, **19**, 1703-1710.
21. Couedel, C., Mills, K.D., Barchi, M., Shen, L., Olshen, A., Johnson, R.D., Nussenzweig, A., Essers, J., Kanaar, R., Li, G.C. *et al.* (2004) Collaboration of homologous recombination and nonhomologous end-joining factors for the survival and integrity of mice and cells. *Genes Dev*, **18**, 1293-1304.
22. Mills, K.D., Ferguson, D.O., Essers, J., Eckersdorff, M., Kanaar, R. and Alt, F.W. (2004) Rad54 and DNA Ligase IV cooperate to maintain mammalian chromatid stability. *Genes Dev*, **18**, 1283-1292.
23. McMahon, M., Frangova, T.G., Henderson, C.J. and Wolf, C.R. (2016) Olaparib, Monotherapy or with Ionizing Radiation, Exacerbates DNA Damage in Normal Tissues: Insights from a New p21 Reporter Mouse. *Mol Cancer Res*, **14**, 1195-1203.
24. Bazalova M, G.E. (2016) MicroCT dose and image quality for in vivo microCT systems. *Unpubl. data*.
25. Peeters, P.J., Fierens, F.L., van den Wyngaert, I., Goehlmann, H.W., Swagemakers, S.M., Kass, S.U., Langlois, X., Pullan, S., Stenzel-Poore, M.P. and Steckler, T. (2004) Gene expression profiles highlight adaptive brain mechanisms in corticotropin releasing factor overexpressing mice. *Brain Res Mol Brain Res*, **129**, 135-150.
26. Hosack, D.A., Dennis, G., Sherman, B.T., Lane, H.C. and Lempicki, R.A. (2003) Identifying biological themes within lists of genes with EASE. *Genome Biol*, **4**.
27. Kramer, A., Green, J., Pollard, J., Jr. and Tugendreich, S. (2014) Causal analysis approaches in Ingenuity Pathway Analysis. *Bioinformatics*, **30**, 523-530.
28. Kabacik, S., Ortega-Molina, A., Efeyan, A., Finnon, P., Bouffler, S., Serrano, M. and Badie, C. (2011) A minimally invasive assay for individual assessment of the ATM/CHEK2/p53 pathway activity. *Cell Cycle*, **10**, 1152-1161.
29. Soille, P. and Vincent, L. (1990) Determining Watersheds in Digital Pictures Via Flooding Simulations. *P Soc Photo-Opt Ins*, **1360**, 240-250.
30. Mujoo, K., Pandita, R.K., Tiwari, A., Charaka, V., Chakraborty, S., Singh, D.K., Hambarde, S., Hittelman, W.N., Horikoshi, N., Hunt, C.R. *et al.* (2017) Differentiation of Human Induced Pluripotent or Embryonic Stem Cells Decreases the DNA Damage Repair by Homologous Recombination. *Stem Cell Reports*, **9**, 1660-1674.
31. Warfel, N.A. and El-Deiry, W.S. (2013) p21WAF1 and tumourigenesis: 20 years after. *Curr Opin Oncol*, **25**, 52-58.
32. Blunt, T., Finnie, N.J., Taccioli, G.E., Smith, G.C., Demengeot, J., Gottlieb, T.M., Mizuta, R., Varghese, A.J., Alt, F.W., Jeggo, P.A. *et al.* (1995) Defective DNA-dependent protein kinase activity is linked to V(D)J recombination and DNA repair defects associated with the murine scid mutation. *Cell*, **80**, 813-823.
33. Jung, D. and Alt, F.W. (2004) Unraveling V(D)J recombination; insights into gene regulation. *Cell*, **116**, 299-311.
34. Shibata, A. and Jeggo, P.A. (2020) Roles for the DNA-PK complex and 53BP1 in protecting ends from resection during DNA double-strand break repair. *J Radiat Res*, **61**, 718-726.
35. Lobrich, M. and Jeggo, P. (2017) A Process of Resection-Dependent Nonhomologous End Joining Involving the Goddess Artemis. *Trends Biochem Sci*, **42**, 690-701.
36. Walker, J.R., Corpina, R.A. and Goldberg, J. (2001) Structure of the Ku heterodimer bound to DNA and its implications for double-strand break repair. *Nature*, **412**, 607-614.
37. Wang, J.L., Duboc, C., Wu, Q., Ochi, T., Liang, S.K., Tsutakawa, S.E., Lees-Miller, S.P., Nadal, M., Tainer, J.A., Blundell, T.L. *et al.* (2018) Dissection of DNA double-strand-break repair using novel single-molecule forceps. *Nature Structural & Molecular Biology*, **25**, 482-+.

38. Wu, Q. (2019) Structural mechanism of DNA-end synapsis in the non-homologous end joining pathway for repairing double-strand breaks: bridge over troubled ends. *Biochem Soc Trans*, **47**, 1609-1619.
39. Riballo, E., Kuhne, M., Rief, N., Doherty, A., Smith, G.C.M., Recio, M.J., Reis, C., Dahm, K., Fricke, A., Krempler, A. *et al.* (2004) A pathway of double-strand break rejoining dependent upon ATM, artemis, and proteins locating to gamma-H2AX foci. *Molecular Cell*, **16**, 715-724.
40. Lu, H., Saha, J., Beckmann, P.J., Hendrickson, E.A. and Davis, A.J. (2019) DNA-PKcs promotes chromatin decondensation to facilitate initiation of the DNA damage response. *Nucleic Acids Res*, **47**, 9467-9479.
41. Stiff, T., O'Driscoll, M., Rief, N., Iwabuchi, K., Lobrich, M. and Jeggo, P.A. (2004) ATM and DNA-PK function redundantly to phosphorylate H2AX after exposure to ionizing radiation. *Cancer Res*, **64**, 2390-2396.
42. Meyer, B., Voss, K.O., Tobias, F., Jakob, B., Durante, M. and Taucher-Scholz, G. (2013) Clustered DNA damage induces pan-nuclear H2AX phosphorylation mediated by ATM and DNA-PK. *Nucleic Acids Research*, **41**, 6109-6118.
43. Savic, V., Yin, B., Maas, N.L., Bredemeyer, A.L., Carpenter, A.C., Helmink, B.A., Yang-Lott, K.S., Sleckman, B.P. and Bassing, C.H. (2009) Formation of Dynamic gamma-H2AX Domains along Broken DNA Strands Is Distinctly Regulated by ATM and MDC1 and Dependent upon H2AX Densities in Chromatin. *Molecular Cell*, **34**, 298-310.
44. Schultz, L.B., Chehab, N.H., Malikzay, A. and Halazonetis, T.D. (2000) p53 Binding protein 1 (53BP1) is an early participant in the cellular response to DNA double-strand breaks. *Journal of Cell Biology*, **151**, 1381-1390.
45. Booth, C., Tudor, G., Tudor, J., Katz, B.P. and MacVittie, T.J. (2012) Acute gastrointestinal syndrome in high-dose irradiated mice. *Health Phys*, **103**, 383-399.

SUPPLEMENTAL FIGURES

Supplemental Table 1. Expression fold change of *CDKN1A* relative to WT.

Genotype	Fold change probe 1	p-value	Fold change probe 2	p-value
RAD54-/-	-1.00	0.9985	1.04	0.8620
DNA-PKCS-/-	1.85	0.1793	1.54	**0.0436**
DNA-PKCS-/-RAD54-/-	2.15	**0.0158**	1.85	**0.0067**

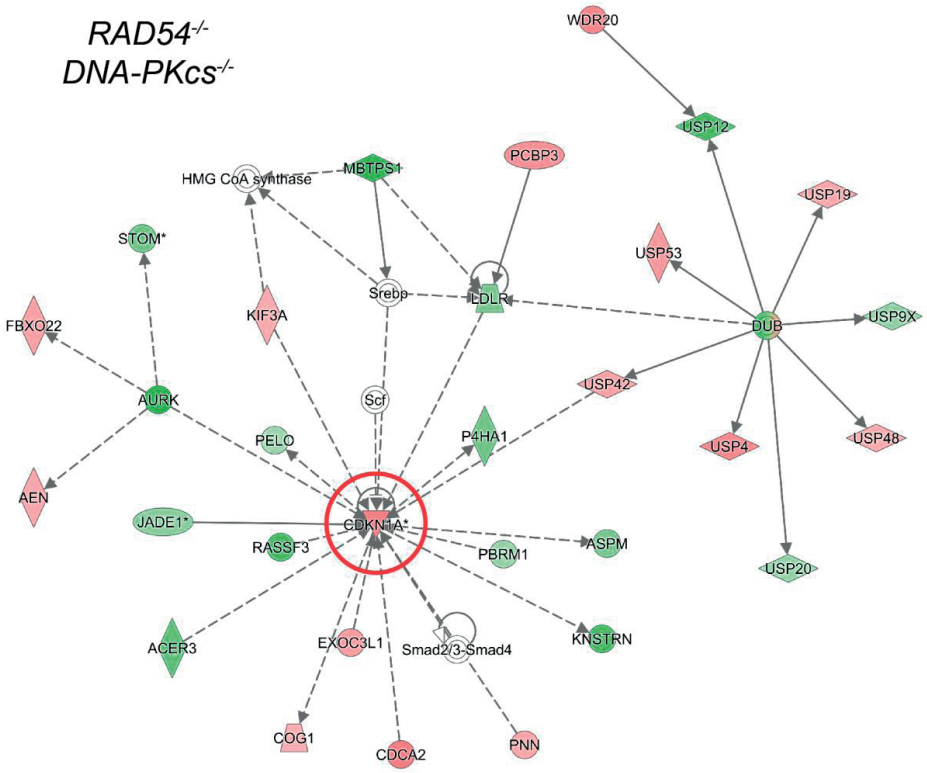

Supplemental figure 1. Ingenuity Pathway Analysis top network in *DNA-PKCS-/-RAD54-/-* mice. Gene expression log ratios: red, upregulated; green, downregulated. Color intensity correlated with the degree of change.

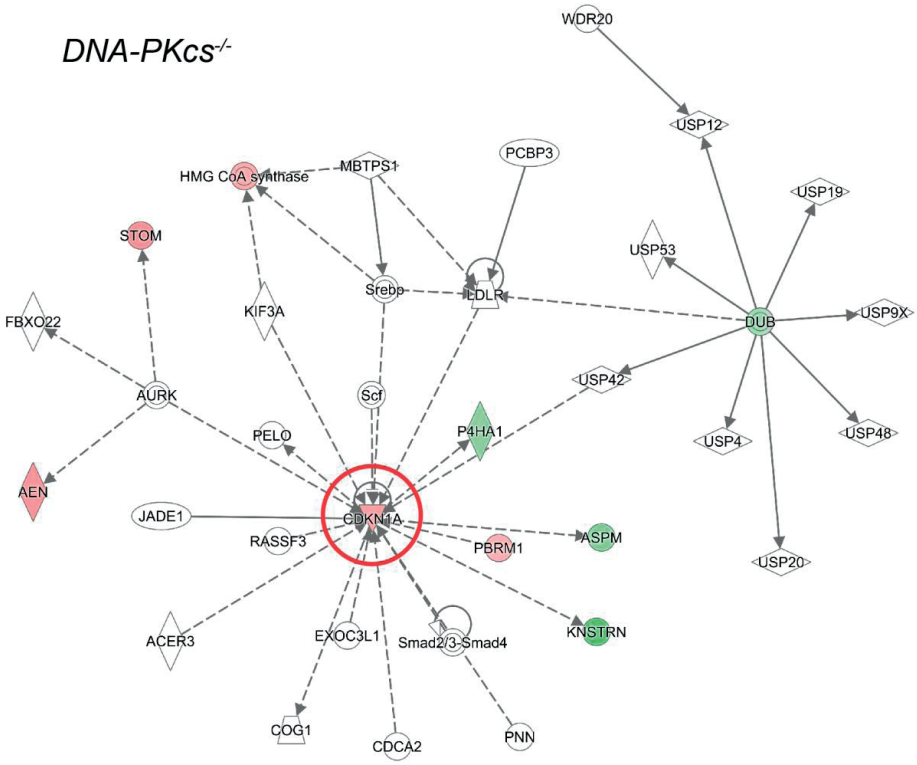

Supplemental figure 2. Ingenuity Pathway Analysis top network in *DNA-PKCS-/-* mice. Gene expression log ratios: red, upregulated; green, downregulated. Color intensity correlated with the degree of change.

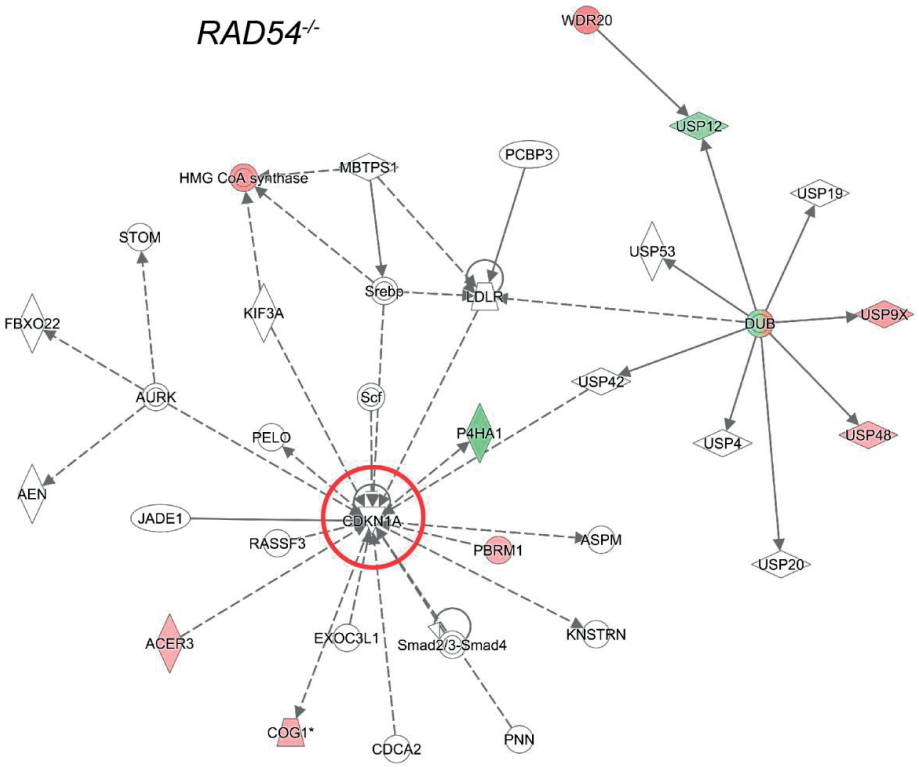

Supplemental figure 3. Ingenuity Pathway Analysis network around CDKN1A in *RAD54-/-* mice. Gene expression log ratios: red, upregulated; green, downregulated. Color intensity correlated with the degree of change.